VNU Journal of Science: Mathematics – Physics, Vol. 40, No. 3 (2024) 31-39

VNU Journal of Science: Mathematics - Physics

Journal homepage: https://js.vnu.edu.vn/MaP

Original Article

A Comparison Study of Photocatalytic Performance of TiO_2 Anatase Phase Prepared from Different Procedures

Vu Hoang Huong, Trinh Thi Loan*

VNU University of Science, 334 Nguyen Trai, Thanh Xuan, Hanoi, Vietnam

Received 26 January 2024
Revised 26 March 2024; Accepted 02 May 2024

Abstract: In this work, three TiO_2 anatase phase samples, labeled as S1, S2, and S3, were synthesized using varying titanium precursors, solvents, and conditions to compare their photocatalytic performances. The structural and morphological properties of the synthesized samples were characterized through X-ray diffraction (XRD), Raman scattering, field emission scanning electron microscopy (FESEM), and transmission electron microscopy (TEM). The obtained results indicated that all samples exhibited an anatase crystalline phase. Sample S1 notably featured nanowires with an average diameter of 38.6 nm. Meanwhile, samples S2 and S3 comprised nanoparticles, each exhibiting unique average sizes of 12.76 nm and 10.11 nm, respectively. The diffuse reflectance spectra reveal that the S3 sample possesses the lowest bandgap, suggesting its potential as the most promising photocatalyst. Additionally, photocurrent response and electrochemical impedance spectroscopy (EIS) were characterized to elucidate the charge transfer mechanisms within the materials. The degradation efficiencies of Rhodamine B (RhB) for samples S1, S2, and S3 were determined to be 17.40%, 17.93%, and 33.04%, respectively, under visible light irradiation. This study provides valuable insights into the criteria for choosing efficient TiO_2 photocatalysts.

Keywords: TiO_2 anatase phase; Nanowires, Nanoparticles; Photocatalysis.

1. Introduction

Titanium dioxide (TiO_2) is a unique semiconductor material with various physical and chemical characteristics. Over the past few decades, TiO_2 nanostructures have garnered significant attention owing to their affordability, non-toxic nature, biocompatibility, and superior chemical stability. Their potential spans across numerous domains, encompassing catalysis, energy storage and harvesting,

---

* Corresponding author.
E-mail address: loan.trinhthi@gmail.com

https//doi.org/10.25073/2588-1124/vnumap.4916

sensing, and various biomedical applications [1, 2]. Titanium dioxide primarily exists in two crystallographic forms: anatase and rutile, each with distinct crystal structures and physical properties. In the field of photocatalysis, the anatase phase of TiO_2 demonstrates better photocatalytic activity compared to the rutile phase, despite the band gap of anatase is larger than the one of rutile [3]. Many researches reveal that, unlike rutile, the anatase phase's greater surface area boosts photocatalytic efficiency by allowing more interaction with reactants [4]. Furthermore, the anatase form exhibits a band structure facilitating indirect band gap transitions, whereas rutile TiO_2 operates as a direct band gap semiconductor [5]. This characteristic of anatase TiO_2 leads to a longer lifetime for the photogenerated electron-hole pairs, thereby increasing the probability of these charge carriers participating in surface reactions. Furthermore, anatase TiO_2 can be synthesized more easily than rutile, as achieving the desired phase in rutile usually involves high-temperature methods [6]. Therefore, the simplicity of production and the enhanced photocatalytic features of the anatase phase make it be a preferred choice for photocatalytic applications.

In this work, the effect of the synthesis process on the photocatalytic performance of TiO_2 anatase phase was analyzed. Three unique samples, futher called S1, S2, and S3, were prepared employing diverse methods, each incorporating distinct precursors, solvents, and conditions of synthesis. The synthesized samples were characterized using XRD, FE-SEM, TEM, Raman, diffuse reflection, PL and UV-visible spectroscopy. The photocatalytic activity of all samples was evaluated under visible light irradiation.

2. Experimental

2.1. Synthesis of TiO_2 Anatase

2.1.1. Synthesis of Sample S1 by Hydrothermal Method

In the experiments, 0.5 g amount of $CO(NH_2)_2$ was dissolved in 80 ml of 10 M solution of NaOH in a beaker. Then, 1 g of TiO_2 powder was introduced to this mixture, with vigorous stirring at room temperature for 30 minutes. The resulting solution was transferred to a teflon-lined steel autoclave, which was put in a drying cabinet and kept at a temperature of 200 ^oC for 24 h and then cooled naturally to room temperature. After that, the precipitate was filtered and washed with HCl, distilled water and ethanol. It was returned to the teflon-lined steel autoclave with 50 ml of distilled water and kept at 160 ^oC for 15 h. Finally, the precipitate was filtered and dried in air at 120 ^oC for 24 h. The product obtained from this procedure was labeled as sample S1.

2.1.2. Synthesis of Sample S2 by a Sol-gel Method

Firstly, 80 ml of ethanol alcohol solution was placed in a beaker. Then, 2 ml solution of $TiCl_4$ (d = 1.73 g/ml) was added dropwise to this solution under stirring at room temperature for 5 min. After, the resulting mixture continued stirring and kept constant at 60 ^oC until a highly viscous gel was formed. The gel was dried in air at 120 ^oC for 24 h and annealed at 600 ^oC for 5 h to yield sample (S2) as a white powder.

2.1.3. Synthesis of Sample S3 by a Hydrothermal Method

TiO_2 nanoparticles were also prepared by hydrothermal method, using $TiCl_4$ solution (d = 1.73 g/ml) as a precursor. Firstly, 20 ml of diluted H_2SO_4 (10%) solution at 5 ^oC was placed in a beaker. The ice bath with this beaker inside was placed on a magnetic stirrer with stirring. Then, 2 ml of $TiCl_4$ solution was slowly added to this solution and stirred for 5 min. After the resulting mixture continued stirring and heated to 60 – 70 ^oC for 1 h, it became a clear solution. Later, concentrated NH_4OH was added drop by drop to the solution until the pH value reached about 7, the precipitate was created. After that, the precipitate was filtered and washed with distilled water. After that, the precipitate was transferred into Teflon-lined steel autoclave, which then was put in a drying cabinet and kept at 220 °C for 24 h. Finally, the precipitate was filtered and dried in air at 120 °C for 24 h, yielding the sample S3.

The all samples fabrication process is briefly presented in Fig. 1.

2.2. Characterizations

The XRD pattens of all samples recorded by using a Siemens D5005 Bruker, Germany X-ray diffractometer with Cu-Kα1 irradiation (λ = 1.54056 Å) are presented for structural analysis of the samples. Raman spectra were measured using LabRam HR800, Horiba spectrometer with 632.8 nm excitation. The samples' morphology was observed using a Nova Nano SEM 450, FEI field emission scanning electron microscope (FESEM) and transmission electron microscope (TEM, JEOL/JEM 1010). Diffuse reflection measurement was carried out on a VARIAN UV-VIS-NIR Cary- 5000 spectrophotometer. The Kubelka-Munk (K-M) function F(R) proportional to the absorption coefficient was calculated using the equation $F(R)=(1-R)^2/(2R)$, where R, K and S are the reflections, the absorption and the scattering coefficient, respectively. The transient photocurrent response and electrochemical impedance spectrum was measured via a CHI 614B electrochemical workstation in the electrolyte of 0.2 M Na_2SO_4. Electrochemical impedance spectroscopy (EIS) spectra were measured in the frequency range of 0.1-100000 Hz. The PL spectra were measured at room temperature using a Fluorolog FL3-22 Jobin Yvon Spex, USA spectrofluorometer with a xenon lamp of 450 W being used as an excitation source.

2.3. Photocatalytic Activity Experiments

Figure 1. Schematic illustration of synthetic procedure for S1, S2 and S3 samples.

Experiments on photocatalytic activity were carried out using a 250 W Osram lamp with a 420 nm cut-off filter [7]. The photocatalytic degradation activity of S1, S2 and S3 was evaluated using RhB as the target molecules. The experiment for photocatalytic degradation was as follows. Under continual stirring, 25 mg of photocatalyst was disseminated in 100 mL RhB solution (10 mg L^{-1}). After a 10-minute ultrasonic treatment, the RhB solution was agitated in the dark for 30 minutes before illumination to achieve adsorption-desorption equilibrium between RhB and photocatalyst [7]. At a predetermined time period (30 minutes), a 5 ml sample was obtained and centrifuged twice to remove sediment. An UV-vis spectrophotometer (Jasco, V-750) was used to measure the concentration of supernatant at 540 nm, which is the typical absorption wavelength of RhB [7].

3. Results and Discussion

3.1. Investigation of Morphology

Fig. 2a presents a FESEM image of S1 sample. Surface morphological studies indicated the formation of nanowires-like structures. The average diameter of TiO_2 nanowires was calculated from the histogram of the diameter sizes as shown in Fig. 2d, with an estimated value of 38.6 nm. Fig. 2b displays a TEM image of S2 sample, and corresponding particle size distribution bar graph with Gaussian fitting is illustrated in Fig. 2e. The TEM image clearly shows that most of particles are irregularly shaped and some are agglomerated. Thisis similar to the morphology of the S3 sample, as shown in Figs. 2c-2f. However, the average particle size of S3 sample, estimated at 10.11 nm, was found to be smaller than that of S2 sample, which was 12.76 nm.

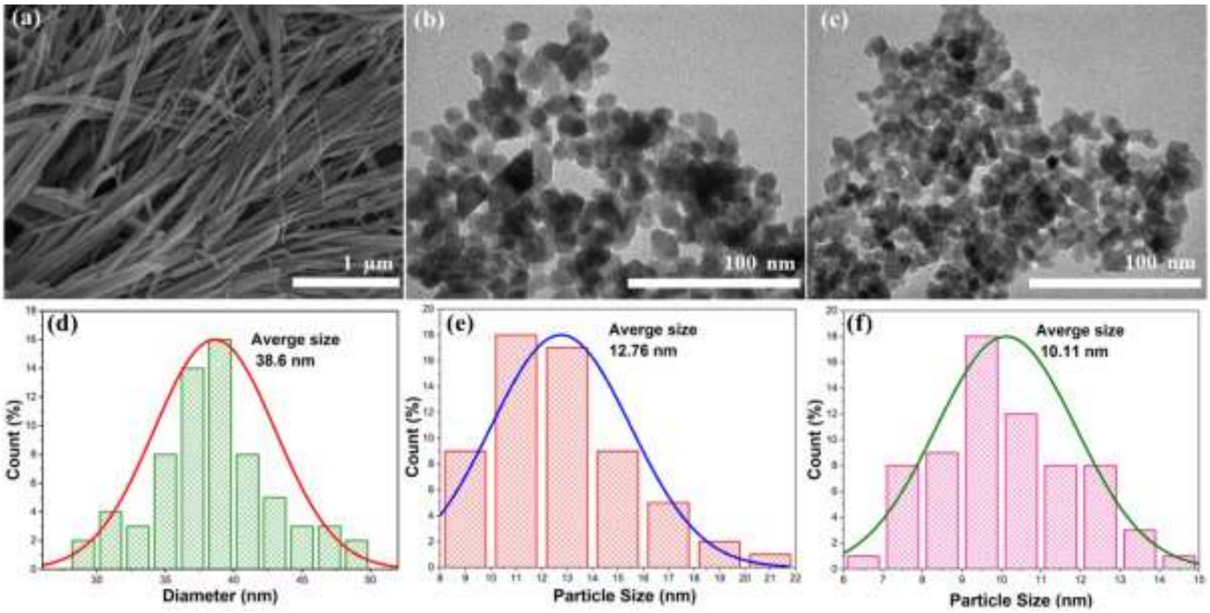

Figure 2. (a-d) FESEM image and diameter size distribution of sample S1, (b-d) TEM image and particle size distribution of sample S2, (c) TEM image and particle size distribution of sample S3.

3.2. Investigation of Structure

Fig. 3a presents XRD patterns of samples S1, S2 and S3, respectively. The peak positions in each sample correspond to the tetragonal structure of single-phase anatase TiO_2, aligning well with the JCPDS card No. 04 – 0477 [8]. Notably, the XRD patterns of samples S1 and S2 exhibit stronger intensity peaks than S3 sample, which indicates that sample S3 has a lower crystallite quality. This can indicate that sample S3 may have defects in the crystal lattice. The lattice parameters of samples were calculated from the XRD patterns using the formula: $d_{hkl} = ((h^2 + k^2)/a^2 + l^2/c^2)^{-1/2}$, where d_{hkl} is interplanar spacing, a and c are lattice parameters. As shown in Table 1, the lattice parameters of the samples, within the margin of error, do not show significant differences. Moreover, they closely approximate the standard values a = b = 3.783 Å and c = 9.510 Å, as per JCPDS card: 04-0477 [8].

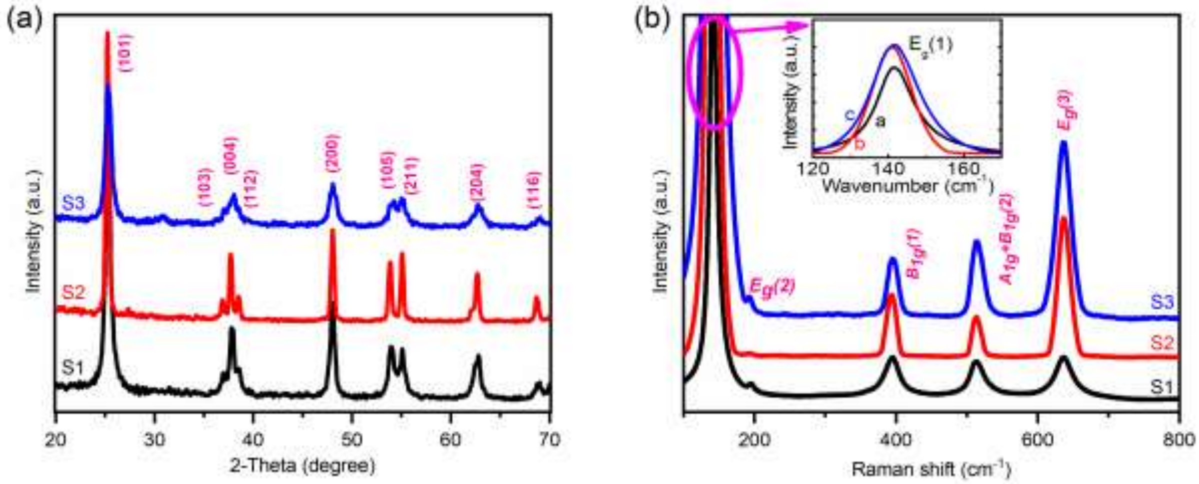

Figure 3. (a) XRD spectra and (b) Raman specra of S1, S2, S3 samples.

Table 1. The lattice parameters of samples S1, S2 and S3

Sample	d_{101} (Å)	d_{200} (Å)	d_{204} (Å)	a = b (Å)	c (Å)
S1	3.5120	1.8920	1.4790	3.783±0.002	9.475±0.027
S2	3.5240	1.8921	1.4808	3.788±0.006	9.550±0.008
S3	3.5200	1.8918	1.4801	3.786±0.003	9.528±0.048

It is well known that TiO_2 anatase phase has tetragonal structure, belongs to space group D_{4h}^{19} ($I4/amd$), and has two TiO_2 units per primitive cell. Group theory predicts six Raman active modes, which are $E_g(1)$ at 144 cm^{1}, $E_g(2)$ at 197 cm^{-1}, $B_{1g}(1)$ at 399 cm^{-1}, $B_{1g}(2)$ at 513 cm^{-1}, A_{1g} at 519 cm^{-1}, and $E_g(3)$ at 638.2 cm^{-1} [9, 10], in which the E_g modes are the symmetric stretching vibrations of O-Ti-O bonds; the B_{1g} modes are the symmetric bending vibrations of O-Ti-O bonds and the A_{1g} mode is the antisymmetric bending vibrations of O-Ti-O bonds [9, 10]. The Raman spectra of samples S1, S2 and S3 are shown in Fig. 3b. It is clear that the frequency of the Raman modes of all the samples are almost the same, each spectrum exhibit modes at approximately 142 cm^{-1} ($E_g(1)$), 195 cm^{-1} ($E_g(2)$) 395 cm^{-1} ($B_{1g}(1)$), 514 cm^{-1} (A_{1g}+$B_{1g}(2)$) and 637 cm^{-1} ($E_g(3)$), with the E_g (1) mode is very intense. The scattering peaks of all the samples correspond to the anatase phase of TiO_2, which is well consistent with the XRD.

3.3. Optical Properties

The diffuse reflectance spectra of the samples are illustrated in Fig. 4a, and the Kubelka-Munk absorption plot is presented in Fig. 4b. The bandgap energies are displayed in Figs. 7(c-f). The band gap energies of samples were calculated using Tauc equation: $\alpha h\nu = A(h\nu - Eg)^n$, where α is the absorption coefficient, $h\nu$ is the photon energy, E_g is the optical band gap, A is a constant which does not depend on the photon energy and *n* is a parameter equal to 1/2 for allowed direct and 2 for allowed indirect transitions [11]. Absorbance coefficient α is proportional to F(R). Here, the bandgap energy of the samples was determined by plotting $[F(R)h\nu]^{1/2}$ versus photon energy *hν*. The E_g value was obtained by extrapolating the linear portion of the plots to the abscissa axis. As shown in Fig. 7(c-e), a perfect fit was obtained for all the samples giving the values of 3.25 eV for sample S1; 3.26 for sample S2 and 3.21 eV for sample S3. These determined values align with those calculated values reported by Daude etal. for the indirect $\Gamma_3 \rightarrow X_1$ (3.19 eV) transitions [12]. They are also in good agreement with the experimental values reported by López et al., as well [13].

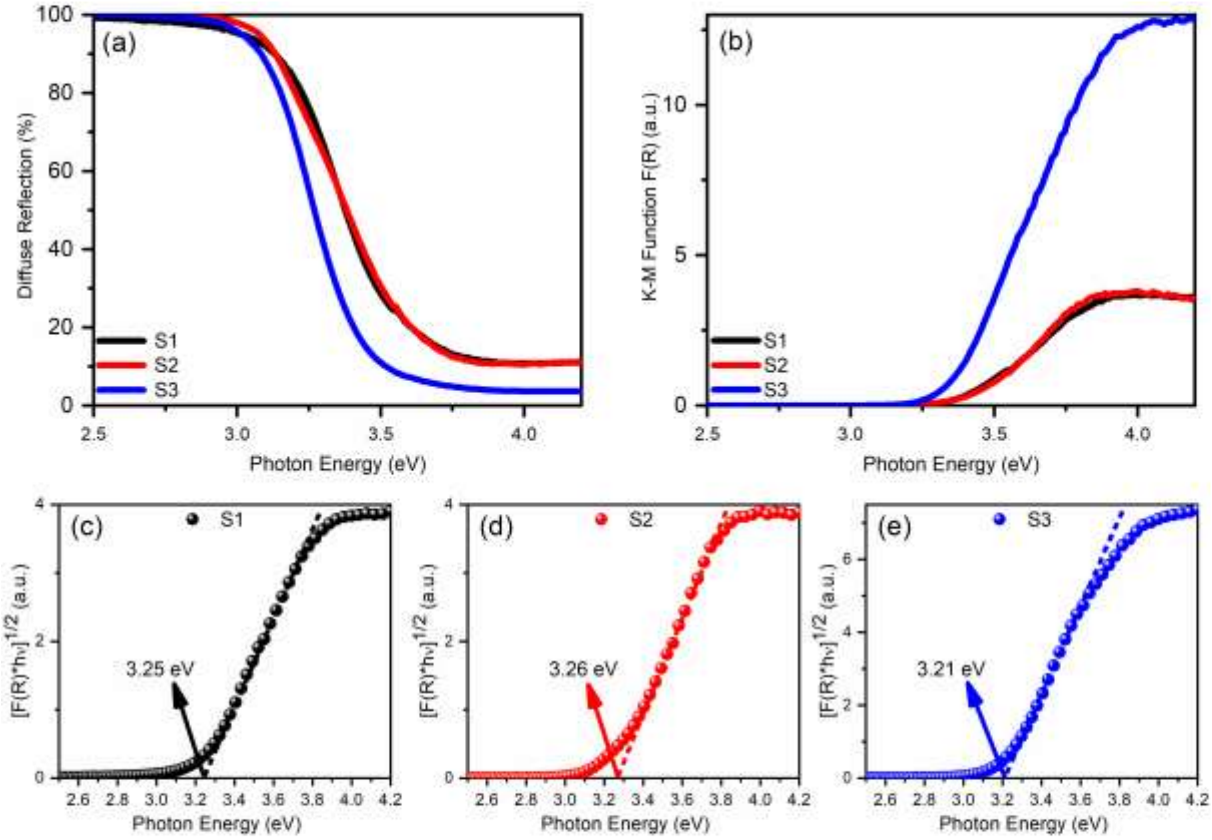

Figure 4. (a) Diffuse reflectance spectra of samples S1, S2 and S3, (b) Kubelka-Munk functions deduced from diffuse reflectance spectra, (c-d-e) plots of $[F(R)h\nu]^{1/2}$ versus photon energy hν.

3.4. Photocatalytic Performance

To evaluate the photocatalytic activity of the synthesized samples, visible light was applied to RhB dye solution. Fig. 5a indicates that the S1 sample exhibits the least photocatalytical activity, while S3 sample demonstrates the highest. The degradation efficiency was calculated using the following formula: The degradation efficiency (%) = $((C_0 - C)/C_0) \times 100\%$, where C_0 represents the initial concentration and C is final concentration of RhB. After 120 minutes of irradiation, the degradation efficiencies for samples S1, S2, and S3 were 17.40%, 17.93%, and 33.04%, respectively. The time-dependent UV-Vis absorption spectra for RhB in the presence of S3, as shown in Fig. 5c, reveal a significant decrease in the absorption peak at 554 nm, which is characteristic of RhB, with increasing irradiation time. No new peaks were observed after 120 minutes of degradation. These results suggest the removal of the ethyl group and the decomposition of the chromophoric structure in the pollutant molecule throughout the photocatalytic degradation process.

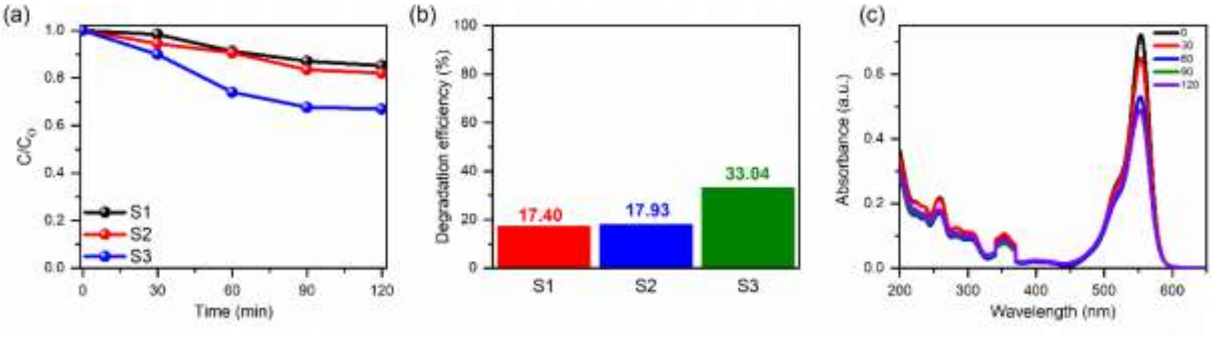

Figure 5. (a) The photocatalytic activities of all samples, (b) Photocatalytic degradation efficiency, and (c) Time dependent UV–vis absorption spectra of RhB of S3 sample.

3.5. Photoelectrochemical Properties

To comprehend photocatalyst activity, the analysis involves examining charge transfer and separation in all samples [14]. Photocurrent response and Electrochemical Impedance Spectroscopy (EIS) tests were performed for this purpose. As demonstrated in Fig. 6a, samples S1 and S2 exhibit a lower photocurrent density compared to sample S3 when exposed to light illumination, which indicates a more efficient separation of photogenerated charge in S3 sample. Additionally, EIS was employed to investigate the charge transfer resistance within the photocatalysts. As illustrated in Fig. 6b, the arc radius for sample S3 is smaller than that of samples S1 and S2. It is known that a smaller arc indicates a reduction in charge transfer resistance [15]. This indirectly reflects that sample S3 possesses a larger conductivity compared to S1 and S2 samples.

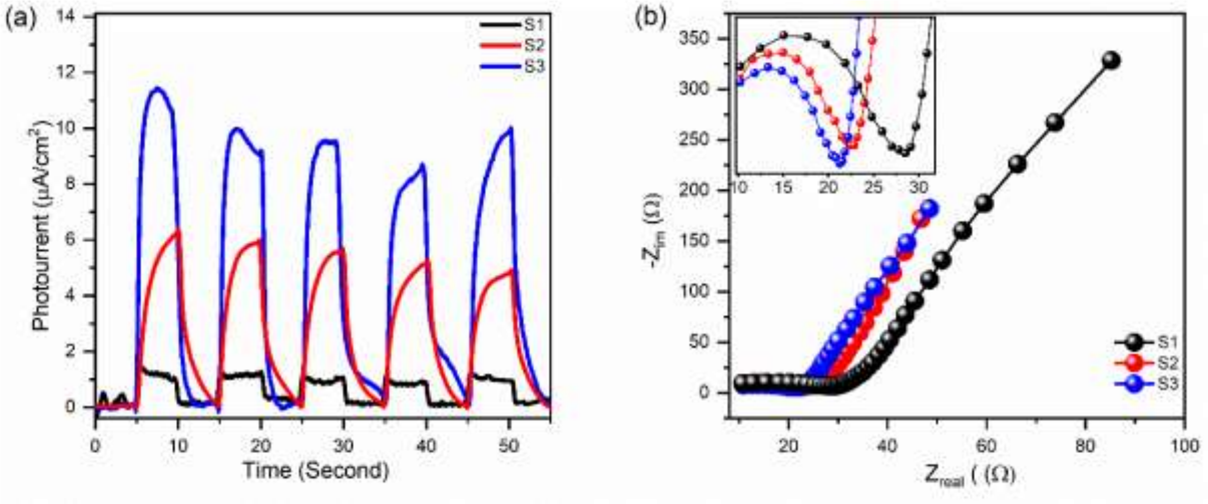

Figure 6. (a) photocurrent response and (b) EIS spectra of S1, S2 and S3 samples under simulated solar light illumination.

3.6. Analysis of the Photocatalytic Reaction Mechanism

Photoluminescence (PL) spectroscopy is an effective technique for analyzing the efficiencies of charge separation and recombination in photocatalysts. When PL intensity decreases, it suggests effective charge separation and slower recombination, which are critical factors in photocatalysis. In Figure 7a, the PL spectra of samples S1, S2, and S3 are presented, excited at 300 nm wavelengths. Notably, sample S1 shows a higher PL intensity compared to samples S2 and S3, which have similar intensities. Contrasting these observations, photocurrent response and EIS results indicate that sample S3 exhibits the highest photocarrier separation efficiency (See Fig. 6). This aligns with its degradation performance, indicating a greater ability for separating photoinduced electron-hole pairs and a lower rate of charge recombination relative to other samples. Additionally, as reported by Kernazhitsky et al., emission peaks observed at 2.76 and 2.84 eV are likely due to the recombination of photoinduced electrons and holes at oxygen vacancies containing trapped electrons, known as F-centers [16].

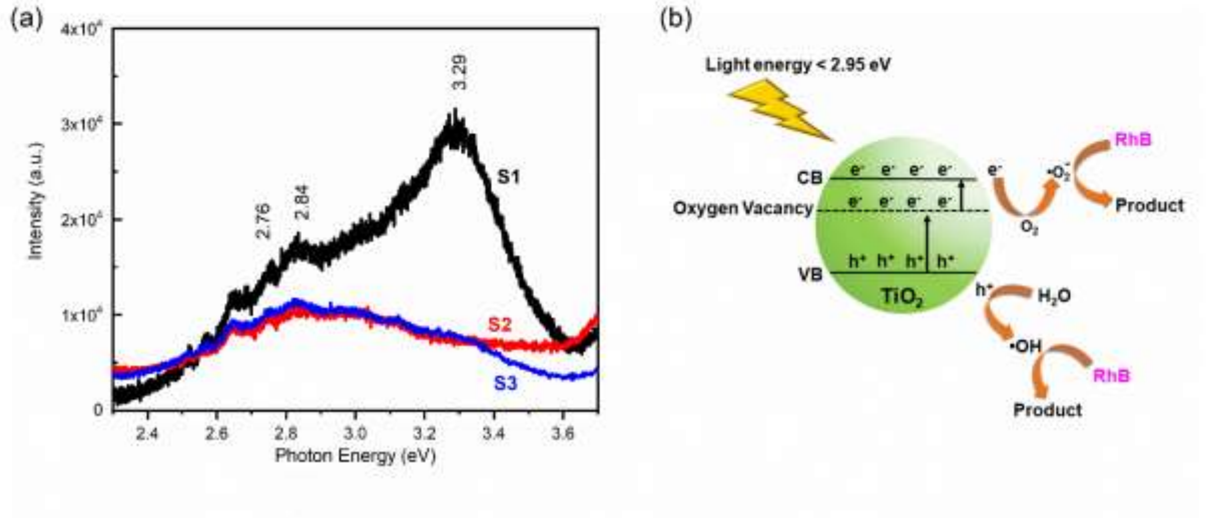

Figure 7. (a) The PL spectra excited by 300 nm wavelengths of samples S1, S2 and S3, (b) Schematic illustration of the photocatalytic mechanism of TiO_2 nano-sized polygon plates with oxygen vacancies.

Based on the results presented above, the photocatalytic mechanism of S3 sample is proposed, as illustrated in Fig. 7b. The presence of oxygen vacancies introduces a new energy level below the conduction band of S3 sample. When exposed to visible light irradiation, these oxygen vacancies effectively capture photogenerated electrons. A portion of these electrons can then migrate to the conduction band, where they react with oxygen molecules to produce the superoxide anion ($\cdot O_2-$). Concurrently, the photogenerated holes interact with water to form hydroxyl radicals ($\cdot OH$). These reactive species, then engage in reactions with RhB molecules, leading to the photodegradation of RhB.

4. Conclusion

In summary, the anatase phase of TiO_2 was successfully synthesized using various methods. TiO_2 nanowire samplew were obtained by hydrothermally treating TiO_2 powder in an alkaline environment (S1), whereas TiO_2 nanoparticles were produced through both hydrothermal and sol-gel methods, respectively called S2 and S3. The band gap energies of S1, S2, and S3 estimated by Tauc plots were of

3.25, 3.26, and 3.21 eV, respectively. Notably, S3 exhibited the highest photodegradation efficiency, achieving 33.04% degradation of RhB dyes within 120 minutes under visible light irradiation. Photocurrent response, EIS, and PL measurements indicated that S3 samples have superior charge separation and recombination efficiencies. These results are highly promising for the future development of TiO_2-based photocatalysts using diverse synthesis methods.

References

[1] S. M. Gupta, M. Tripathi, A Review of TiO_2 Nanoparticles, Chinese Sci Bull, Vol. 56, No. 16, 2011, pp. 1639-1657, https://doi.org/10.1007/s11434-011-4476-1.

[2] S. Reghunath, D. Pinheiro, S. D. KR, A Review of Hierarchical Nanostructures of TiO_2: Advances and Applications, Applied Surface Science Advances Vol. 3, 2021, pp. 100063, https://doi.org/10.1016/j.apsadv.2021.100063.

[3] T. Luttrell, S. Halpegamage, J. Tao, A. Kramer, E. Sutter, M. Batzill, Why is Anatase A Better Photocatalyst than Rutile? - Model Studies on Epitaxial TiO_2 Films, Scientific Reports, Vol. 4, 2014, pp. 4043, https://doi.org/10.1038/srep04043.

[4] J. N. Wilson, H. Idriss, Effect of Surface Reconstruction of TiO_2 (001) Single Crystal on the Photoreaction of Acetic Acid, J. Catal., Vol. 214, 2003, pp.46-52, https://doi.org/10.1016/S0021-9517(02)00172-0.

[5] M. Xu, Y. Gao, E. M. Moreno, M. Kunst, M. Muhler, Y. Wang, H. Idriss, C. Wöll, Photocatalytic Activity of Bulk TiO_2 Anatase and Rutile Single Crystals Using Infrared Absorption Spectroscopy, Phys. Rev. Lett., Vol. 106, 2011, pp. 138302, https://doi.org/10.1103/physrevlett.106.138302.

[6] P. Lavudya, H. Pant, V. V. S. S. Srikanth, R. Ammanabrolu, Mesoporous and Phase Pure Anatase TiO_2 Nanospheres for Enhanced Photocatalysis, Inorg. Chem. Commun., Vol. 152, 2023, pp. 110699, https://doi.org/10.1016/j.inoche.2023.110699.

[7] V. H. Huong, Construction of Sn_3O_4/g-C_3N_4 Composite with Enhanced Photocatalytic Activities Under Visible Light Irradiation, Vol. 39, No. 1, 2023, https://doi.org/10.25073/2588-1124/vnumap.4761.

[8] T. T. Loan, N. N. Long, Synthesis and Characterization of Anatase TiO_2:Cu^{2+} Powders Prepared Via a Sol-gel Technique, Vol. 34, No. 3, 2018, https://doi.org/10.25073/2588-1124/vnumap.4272.

[9] O. Frank, M. Zukalova, B. Laskova, J. Kurti, J. Koltaib, L. Kavan, Raman Spectra of Titanium Dioxide (Anatase, Rutile) with Identified Oxygen Isotopes (16, 17, 18), Phys. Chem. Chem. Phys., Vol. 14, 2012, pp. 14567-14572, https://doi.org/10.1039/C2CP42763J.

[10] T. Ohsaka, F. Izumi, Y. Fujiki, Raman Spectrum of Anatase, TiO_2, Vol. 7, No. 6, 1978, pp. 321-324, https://doi.org/10.1002/jrs.1250070606.

[11] B. D. Viezbicke, S. Patel, B. E. Davis, D. P. Birnie, Evaluation of the Tauc Method for Optical Absorption Edge Determination: ZnO Thin Films As A Model System, Phys. Status Solidi B, Vol. 252, 2015, pp. 1700-1710, https://doi.org/10.1002/pssb.201552007.

[12] N. Daude, C. Gout, C. Jouanin, Electronic Band Structure of Titanium Dioxide, Phys. Rev. B, Vol. 15, 1977, pp. 3229-3235, https://doi.org/10.1103/PhysRevB.15.3229.

[13] R. López, R. Gómez, Band-gap Energy Estimation from Diffuse Reflectance Measurements on Sol–Gel and Commercial TiO_2: A Comparative Study, Vol. 61, No. 1, 2012, pp. 1-7, http://dx.doi.org/10.1007/s10971-011-2582-9.

[14] V. H. Huong, T. T. Loan, K. P. Pham, M. N. Ha, Q. H. Nguyen, Y. R. Ma, A. B. Ngac, V. C. Nguyen, Unveiling the Synergistic Interplay of Appropriate Oxygen Vacancies and S-Scheme Heterojunction Structures in OVs-TiO_2/g-C_3N_4 Catalyst for Efficient RhB Photodegradation and H_2 Production, J. Alloys Compd., Vol. 972, 2024, pp. 172722, https://doi.org/10.1016/j.jallcom.2023.172722.

[15] M. Zhang, M. Arif, Y. Dong, X. Chen, X. Liu, Z-scheme TiO_{2-x}@$ZnIn_2S_4$ Architectures with Oxygen Vacancies-Mediated Electron Transfer for Enhanced Catalytic Activity Towards Degradation of Persistent Antibiotics, Colloids Surf. A: Physicochem. Eng., Vol. 649, 2022, pp. 129530, https://doi.org/10.1016/j.colsurfa.2022.129530.

[16] L. Kernazhitsky, V. Shymanovska, T. Gavrilko, V. Naumov, L. Fedorenko, V. Kshnyakin, J. Baran, Room Temperature Photoluminescence of Anatase and Rutile TiO_2 Powders, J. Lumin, Vol. 146, 2014, pp. 199-204, https://doi.org/10.1016/j.jlumin.2013.09.068.